Biogenesis and Topology of the Secretory $Na^+-K^+-2Cl^-$ Cotransporter (NKCC1) Studied in Intact Mammalian Cells†

Tudevdagva Gerelsaikhan,‡ Most. Nahid Parvin, and R. James Turner*

Membrane Biology Section, Gene Therapy and Therapeutics Branch, National Institute of Dental and Craniofacial Research, National Institutes of Health, DHHS, Bethesda, Maryland 20892

Received June 6, 2006; Revised Manuscript Received July 27, 2006

ABSTRACT: The "secretory" $Na^+-K^+-2Cl^-$ cotransporter (NKCC1) is a member of a small gene family with nine homologues in vertebrates. Of these, seven are known to be electroneutral chloride transporters. These transporters play a number of important physiological roles related to salt and water homeostasis and the control of intracellular chloride levels. Hydropathy analyses suggest that all of these transporters have a similar transmembrane topology consisting of relatively large intracellular N and C termini and a central hydrophobic domain containing 12 membrane-spanning segments (MSSs). In recent experiments from our laboratory [Gerelsaikhan, T., and Turner, R. J. (2000) *J. Biol. Chem. 275*, 40471−40477], we employed an *in vitro* translation system to confirm that each of the putative MSSs of NKCC1 was capable of membrane integration in a manner consistent with a 12 MSS model. Here, we extend that work to the study of the biogenesis of NKCC1 in intact cells. We employ a truncation mutant approach that allows us to monitor this process quantitatively as successive MSSs are synthesized. While the results presented here confirm the 12 MSS model, they also indicate that the integration of NKCC1 into the membrane does not occur via a simple cotranslational process. In particular, we demonstrate that two MSSs, the second and sixth, require the presence of downstream sequence to efficiently integrate into the membrane.

The "secretory" $Na^+-K^+-2Cl^-$ cotransporter (NKCC1)[1] is widely expressed in vertebrate tissues, where it mediates the electroneutal transport of Na^+, K^+, and Cl^- across cell membranes with a coupling stoichiometry of $1Na^+/1K^+/2Cl^-$ (*1*, *2*). In secretory epithelia, NKCC1 provides the concentrative Cl^- entry step at the basolateral membrane that drives transepithelial salt and water movements. In other cell types, it has been shown to be involved in volume regulation and the control of intracellular Cl^- levels. Traditional physiological approaches together with knockout mouse models have demonstrated important functional roles for NKCC1 in epithelial Cl^- transport, hearing, olfaction, pain perception, spermatogenesis, and maintenance of blood pressure and vascular tone (*1*−*11*).

NKCC1 belongs to a small gene family with nine homologues in vertebrates (*2*). Of these, seven are known to be electroneutral cation-chloride cotransporters (CCCs); in addition to NKCC1, these include an "absorptive" $Na^+-K^+-2Cl^-$ cotransporter isoform (NKCC2), a Na^+-Cl^- cotransporter (NCC), and four K^+-Cl^- cotransporter isoforms (KCC1, KCC2, KCC3, and KCC4). The function of the remaining two vertebrate homologues remains uncertain. Hydropathy analyses indicate that all of the vertebrate CCCs have a similar general structure consisting of large hydrophilic N and C termini (15−35 and ∼50 kDa, respectively) on either side of a central hydrophobic domain (∼50 kDa) predicted to contain 12 membrane-spanning segments (MSSs). Strong experimental evidence indicates that the N and C termini of NKCC1 are intracellular (reviewed in ref *12*). In addition, sites of N-linked glycosylation have been identified between the seventh and eighth putative MSSs of NKCC1, NKCC2, and NCC (*13*−*15*), demonstrating that this loop is extracellular.

The integration of membrane proteins into the bilayer of the endoplasmic reticulum (ER) has been shown to occur with the aid of a large protein complex referred to as the *translocon* (*16*−*18*). The functional core of this complex is a transmembrane aqueous channel sufficiently large to accommodate one or more MSSs. Ribosomes that are synthesizing membrane proteins associate with the translocon in such a way that successive MSSs are fed into this channel, where they are recognized and ultimately transferred laterally into the lipid bilayer in their proper transmembrane orientation (*16*−*19*). In the simplest case, each MSS of a polytopic membrane protein is sequentially recognized, oriented, and integrated into the membrane by the translocon as it is synthesized. Thus, for a protein such as NKCC1 whose N terminus is cytosolic, the first MSS is recognized and inserted into the membrane with its N terminus facing the cytoplasmic side of the ER and its C terminus toward the ER lumen (N_{cyt}/C_{lum}). A MSS in this configuration is referred to as a *(type II) signal anchor sequence*. The amino acids in the nascent

† This research was supported by the Intramural Research Program of the NIH, National Institute of Dental and Craniofacial Research.

* To whom correspondence should be addressed: Building 10, Room 1A01, 10 Center Drive, MSC 1190, National Institutes of Health, Bethesda, MD 20892-1190. Telephone: (301) 402-1060. Fax: (301) 402-1228. E-mail: rjturner@nih.gov.

‡ Present address: Department of Psychiatry, Health Sciences Center, SUNY, Stony Brook, NY 11794-8101.

[1] Abbreviations: NKCC, $Na^+-K^+-2Cl^-$ cotransporter; MSS, membrane-spanning segment; NCC, Na^+-Cl^- cotransporter; KCC, K^+-Cl^- cotransporter.

10.1021/bi061126x CCC: $33.50
Published on Web 09/07/2006

chain that follow this signal anchor sequence are then extruded through the translocon into the interior of the ER as they are synthesized. This translocation process is subsequently stopped by the appearance of a second MSS that acts as a *stop transfer sequence* by associating with and being retained by the translocon complex in the opposite orientation (N_{lum}/C_{cyt}) to that of the preceding signal anchor. The amino acids in the nascent chain that follow this stop transfer sequence will then remain on the cytosolic side of the membrane until the appearance of a new signal anchor sequence and so on.

Although the simple process of cotranslational integration described above can account for the membrane integration of many polytopic membrane proteins, significantly more complex scenarios have been well-documented. In particular, it has been shown that the orientation and/or integration of a potential MSS can be influenced by neighboring MSSs or by the structure or charge of its flanking regions (*17*−*19*). It is also thought that multiple MSSs can occupy the translocon channel simultaneously, where they can interact with one another and orient according to topogenic signals encoded into the MSSs themselves or their flanking sequences. In some cases, multiple MSSs may also exit the translocon into the bilayer *en bloc* (*20*).

In a recent publication from our laboratory (*12*), we employed an *in vitro* translation system to assay for the signal anchor and stop transfer activities of the 12 putative MSSs of NKCC1. These experiments yielded results consistent with a 12 MSS model. In the present paper, we extend these studies using a truncation mutant approach that allows us to quantitatively monitor the biogenesis of NKCC1 in intact mammalian cells (*21*, *22*). While the results presented here confirm the 12 MSS model, they also indicate that the integration of NKCC1 into the membrane does not occur via a simple cotranslational process.

MATERIALS AND METHODS

DNA Constructs. Segments of the rat NKCC1 sequence were cloned into the mammalian expression vector pEGFP-β, whose construction has been described previously (*21*). This vector drives the expression of a fusion protein consisting of the enhanced green-fluorescent protein (EGFP), followed by *Bgl* II and *Hin*d III restriction sites for the insertion of an additional sequence, and then a C-terminal glycosylation tag. The segments of NKCC1 indicated in the text and/or the captions in the figures were amplified by polymerase chain reaction (PCR) and cloned directly into pEGFP-β by standard methods. The rat parotid NKCC1 (*23*) was used as a template for the PCR reactions. The PCR primers, incorporating 5′ and 3′ *Bgl* II and *Hin*d III sites, respectively, were designed essentially as reported in previous studies from our laboratory (*21*). In all fusion protein constructs, the amino acids SerAspLeu and GlySerPhe, coded (in part) by *Bgl* II and *Hin*d III, respectively, flanked the NKCC1 inserts in pEGFP-β. All NKCC1 inserts began at D261. All PCR products were sequenced to confirm that they were correct.

Growth and Transient Transfection of HEK-293T Cells. HEK-293T cells obtained from American Type Culture Collection (ATCC) were cultured in Dulbecco's modified Essential medium supplemented with 2 mM glutamine, 100 μg/mL each of penicillin and streptomycin (all from Biofluids), and 10% heat-inactivated fetal bovine serum (GibcoBRL). Cells were grown in 10 cm plastic dishes in a humidified incubator at 37 °C and 5% CO_2 and subcultured every 2−3 days. Subconfluent (~80%) HEK-293T monolayers were transiently transfected overnight (19−24 h) with the expression vectors indicated using Polyfect (Qiagen) according to the instructions of the manufacturer.

Preparation of Particulate and Membrane Fractions from HEK-293T Cells. Particulate and membrane fractions from transiently transfected HEK-293T cells were obtained as previously described (*22*). Briefly, cells were washed in phosphate-buffered saline (PBS) and then homogenized in ice-cold TEEA buffer consisting of 20 mM Tris-HCl at pH 8.0, 1 mM ethylenediaminetetraacetic acid (EDTA), 3 mM ethylene glycol bis(2-aminoethyl ether)-*N*,*N*,*N*′,*N*′-tetraacetic acid (EGTA), 300 μM AEBSF (ICN), 10 μM leupeptin, 10 μM pepstatin A, and 2.5 μg/mL aprotinin (all from Roche). This material was centrifuged at 1000*g* for 10 min, and the supernate was saved. The pellet was resuspended in TEEA buffer, rehomogenized, and centrifuged as before. The combined supernates from these two homogenization steps were centrifuged at 100000*g* for 30 min, and the resulting "particulate fraction" was resuspended in TEEA buffer, snap-frozen, and stored above liquid nitrogen (the protein concentration was typically 5−10 mg/mL, measured using the Bio-Rad protein assay kit with bovine IgG as the standard).

The "membrane fraction" was prepared from the above particulate fraction by an alkaline floatation step as follows. An aliquot of the particulate fraction containing 50−100 μg of protein was diluted to 25 μL with water, and 25 μL of 200 mM Na_2CO_3 (pH 12.0) was added. This mixture was incubated on ice for 30 min and then mixed with 90 μL of 2.5 M sucrose in 100 mM Na_2CO_3. Next, 50 μL of 1.25 M sucrose and 50 μL of 0.25 M sucrose, both containing 0.2 mM EDTA and 10 mM Tris-HCl (pH 8.0), were overlaid on the alkaline mixture, and the tube was centrifuged at 100000*g* for 60 min in a Beckman TL100 ultracentrifuge equipped with a TLA100.3 rotor. The 0.25 and 1.25 M sucrose layers and the interface between the 1.25 M sucrose layer and the alkaline mixture were recovered as the membrane fraction.

Deglycosylation of the Membrane Fraction. Aliquots of the above membrane fraction were treated with the peptide *N*-glycosidase F (PNGase F; New England Biolabs) as follows. A 10 μL aliquot of the membrane fraction was diluted to 20 μL in 50 mM sodium phosphate (pH 7.5), 0.5% sodium dodecyl sulfate (SDS), and 1% β-mercaptoethanol (final concentrations) and incubated at room temperature for 10 min. Next, 2.22 μL of 10% NP-40 and 1 μL (1000 units) of PNGase F were added, and this mixture was incubated at 37 °C for 2 h. In control samples, PNGase F was substituted by its storage buffer (20 mM Tris-HCl at pH 7.5, 50 mM NaCl, 5 mM Na_2EDTA, and 50% glycerol).

Western Blotting and Analysis. SDS−polyacrylamide gel electrophoresis (PAGE) was carried out on 4−20% Tris/glycine Ready Gels (Bio-Rad) using a sample buffer containing 0.5% SDS. Western blotting using rabbit anti-GFP polyclonal antibody (Molecular Probes) was carried out as previously described (*21*). Samples were not boiled before SDS−PAGE because previous results indicated that this antibody is mainly directed against nondenatured EGFP. For

A

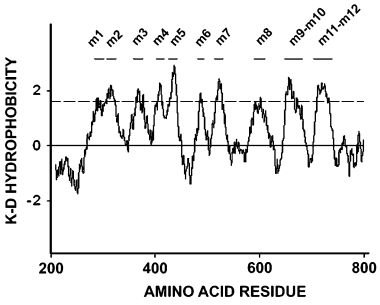

B

```
                                                    ..... DAVVTYTAES KGVVKFGWIK
281  GVLVRCMLNI WGVMLFIRLS WIV*GQAGIGL SVLVIAMATV VTTITGL*STS AIATNGFVRG* GGAYYLISRS
                    m1                  m2
351  LGPEFGGAIG LIFAFANAVA VAMYVVGFAE TVVELLKEHS ILMIDEINDI RIIGAITVVV LLGISVAGME
                  m3                                                    m4
421  WEAKAQIVLL VILLLAIADF VIG*TFISLDS KKPKGFFGYK SEIFSENFGP DFREEETFFS VFAIFFPAAT
                m5                                                    m6
491  GILAGANISG DLADPQSAIP KGTLLAILIT TVVYIGIAVS VGSCVVRDAT GNVNDTITTE LTNCTSAACK
                          m7
561  LNFDFSYCES NTCSYGLMNN FQVMSMVSGF APLISAGIFS ATLSSALASL VSAPKIFQAL CKDNIYPAFQ
                                    m8
631  MFAKGYGKNN EPLRGYILTF LIALGFILIA ELNVIAPIIS NFFLASYALI NFSVFHASLA KSPGWRPAFK
                        m9                  m10
701  YYNMWISLTG AILCCIVMFV INWWAALLTY VIVLGLYIYV TYKKPDVNWG SSTQALTYLS .....
                  m11                 m12
```

FIGURE 1: Hydropathy plot, amino acid sequence, and predicted positions of MSSs in the central hydrophobic domain of NKCC1. (A) Hydropathy plot for the central hydrophobic domain of NKCC1, plotted according to Kyte and Doolittle (*36*) using a 19 amino acid window. The dashed line indicates an average hydropathy of 1.6/residue, the value suggested by Kyte and Doolittle as the threshold for membrane insertion. Predictions of the NKCC1 topology obtained using a number of other methods developed over the past decade are given in ref *12*. (B) *Approximate* positions of the 12 putative MSSs of NKCC1 are indicated. The amino acids marked with asterisks indicate the truncation points of the NKCC1 inserts in pEGFP-β described in the paper.

Western blots using a monoclonal antibody directed against the β subunit of the gastric H,K-ATPase (Research Diagnostics), samples were boiled for 3 min before SDS−PAGE. For these blots, all incubations were carried out in TBST (100 mM Tris-HCl at pH 7.4 containing 0.9% NaCl and 0.05% Tween 20). Blocking was carried out in TBST plus 1% bovine serum albumin (BSA) as was the incubation with the primary (overnight at 1:2000 dilution) and secondary (horseradish-peroxidase-conjugated rabbit anti-mouse IgG at 1:5000 dilution) antibodies. For all Western blots, detection was carried out using the ECL kit from Amersham and quantitation was done using Imagequant software (Molecular Dynamics). Quantitative results shown are means ± standard error (SE) for three or more independent experiments.

RESULTS AND DISCUSSION

Rationale and Approach. In Figure 1, we show a classical hydropathy plot (A) and the amino acid sequence (B) of the central hydrophobic domain of rat NKCC1. The approximate positions of the 12 (putative) MSSs, labeled m1, m2, ..., m12, are indicated in both A and B. As already mentioned, there is very strong evidence that the N and C termini of NKCC1 (i.e., the sequence upstream of m1 and downstream of m12) are intracellular and it has been shown that the native sites of N-linked glycosylation on this protein are located in the hydrophilic loop between m7 and m8 (specifically N544 and/or N553), so that this loop is extracellular. In our previous studies (*12*), we established that each of the putative MSSs, m1−m12, exhibited the ability to insert into isolated microsomes *in vitro* in a manner consistent with a 12 MSS model, namely, that all odd-numbered segments (m1, m3, ..., m11) exhibited signal anchor activity and all even-numbered segments (m2, m4, ..., m12) exhibited stop transfer activity. However, these experiments were limited in that (i) they were difficult to quantitate; therefore, we were unable to confidently determine how strongly the individual segments actually integrated into the microsomal membrane, and (ii) in our hands, it was not possible to obtain efficient expression and membrane integration of constructs containing more than two putative MSSs, making it impossible to study potential effects of a more distant sequence or, more generally, NKCC1 biogenesis.

In this paper, we have used a truncation mutant approach, recently developed in our laboratory (*21*), to explore the topology and biogenesis of NKCC1 in intact cells. This method circumvents the above limitations because results can be easily quantitated and very long constructs incorporating multiple MSSs can be studied. In addition, it has the added advantage of utilizing living cells where all of the membrane integration machinery is necessarily completely intact. In this approach, portions of the NKCC1 sequence beginning at D261 and containing one or more putative MSSs were ligated into the mammalian expression vector pEGFP-β (see the Materials and Methods) between EGFP and the extracellular tail (177 amino acids) of the β subunit of the rabbit gastric H,K-ATPase, a glycosylation tag. This latter sequence contains five consensus sites for N-linked glycosylation (*24*); when translocated into the interior of the ER, this tag acquires ~14 kDa of apparent molecular weight because of glycosylation (*12*, *21*, *22*), an increase that is easily detected on SDS−PAGE. The use of this glycosylation tag in membrane protein topology and biogenesis studies is now well-established (*12*, *21*, *22*, *24*−*26*).

EGFP in these constructs provides a convenient marker for fusion protein detection on Western blots. In addition, this N-terminal EGFP moiety is expected to act as a "cytosolic anchor" that constrains the N-terminal end of the fusion protein to remain in the cytosol. This is because the synthesis and folding of EGFP into a stable compact structure precedes the appearance of the MSSs of the fusion protein from the ribosome, and the stably folded EGFP structure is too large to enter the translocon channel and pass into the lumen of the ER (*27*, *28*). In this way, EGFP mimics the N terminus of NKCC1. It is worth mentioning that in our initial experiments we attempted to include the complete N terminus of NKCC1 in our constructs instead of EGFP, but these truncated proteins exhibited widely varying levels of expression and degradation (data not shown), making data analysis difficult. We typically do not observe these undesirable effects with our EGFP fusion proteins. Because EGFP is known to be a very stable molecule that is well-tolerated by mammalian cells, we speculate that some of this stability may be inherited by EGFP fusion proteins as well; however, it is also possible that there are sequences within the N terminus of NKCC1 that target truncated transporters for destruction. We have not explored these possibilities further.

Membrane Integration of m1, m2, m3, and m4. In Figure 2, we show the results of a series of experiments where portions of the NKCC1 sequence including m1 (V303), m1 and m2 (I362), m1−m3 (F378), and m1−m4 (G418) were expressed as EGFP/β-subunit fusion proteins in HEK-293T cells (note that the constructs V303, F378, and G418 end near the C-terminal ends of m1, m3, and m4, respectively,

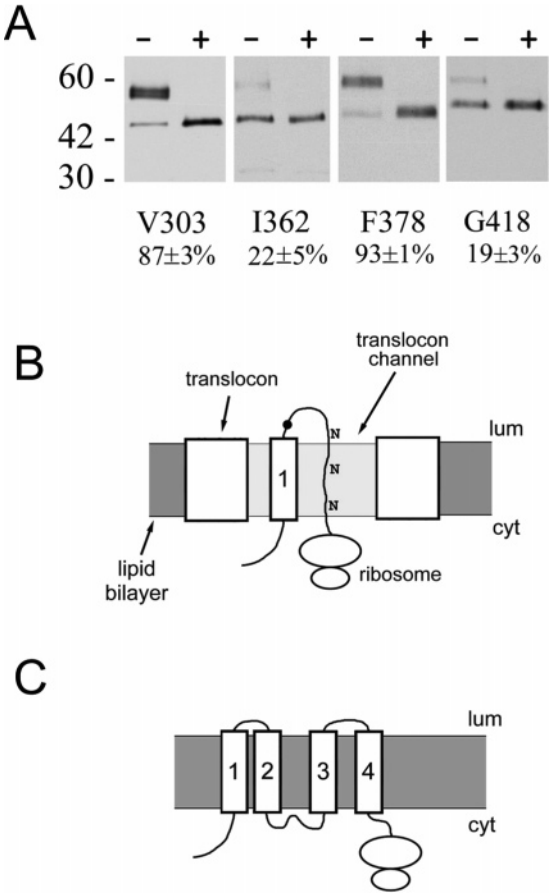

FIGURE 2: Membrane integration of m1−m4 of NKCC1. (A) Typical Western blots of membrane fractions prepared from HEK-293T cells transfected with the truncation mutants indicated. Membranes were treated with (+) or without (−) PNGase F and probed with an antibody against EGFP. All procedures are described in the Materials and Methods. For each construct, the density of the glycosylated band expressed as a percentage of the total recombinant protein (glycosylated band plus unglycosylated band) is indicated below the blot. (B) Schematic representation of m1 within the translocon channel during the synthesis of the recombinant protein V303. See the text for details. (C) Schematic representation of the topology of m1−m4 of NKCC1. See the text for a discussion.

while I362 includes the loop between m2 and m3; the significance of designing I362 in this way will be made clear shortly). In each of the panels in Figure 2A, we show the results of a typical experiment where the membrane fraction from HEK-293T cells, transiently transfected with the truncation mutant indicated, was treated with (+) or without (−) PNGase F (see the Materials and Methods). These membrane fractions were run on SDS−PAGE and probed by Western blotting with an antibody against EGFP to determine the extent of glycosylation of the β subunit and thus its location inside or outside the ER lumen. The percentage of glycosylated recombinant protein is indicated below each panel. The mutant truncated near the end of m1 (V303) is highly glycosylated (~90%), indicating that the glycosylation tag has been translocated into the lumen of the ER and, thus, that m1 is recognized by the translocon channel as a signal anchor sequence and integrated into the ER membrane in a N_{cyt}/C_{lum} orientation. Figure 2B shows a schematic representation of m1 within the translocon channel during the synthesis of the recombinant protein V303. The black dot at the C-terminal end of m1 indicates the end of the NKCC1 sequence (at V303), and the Ns represent glycosylation sites on the glycosylation tag as it passes through the translocon toward the luminal space. In this representation, the glycosylation tag is still being synthesized by the ribosome and thus is still attached to it. Note that the translocon, translocon channel, and m1 (assumed to be α-helical) have been drawn approximately to scale (diameters of ~10, ~5, and ~1 nm, respectively), while the ribosome is drawn at ~1/10 scale (actual diameter of ~25 nm); in subsequent diagrams of this type, a depiction of the translocon has been omitted for simplicity.

Returning to Figure 2A, we see that the mutant truncated at I362 is only weakly glycosylated (~20%), indicating that its C-terminal end is cytosolic and, thus, that there is a stop transfer sequence following m1 in this construct, presumably the hydrophobic region m2 (Figure 1). The mutants truncated near the ends of m3 (F378) and m4 (G418) are highly glycosylated (~90%) and weakly glycosylated (~20%), respectively, indicating that m3 acts as a signal anchor sequence and m4 acts as a stop transfer sequence in these constructs.

When the results illustrated in Figure 2A are taken together with the hydropathy profile shown in Figure 1A, they suggest that regions m1−m4 of NKCC1 integrate into the membrane as illustrated in Figure 2C. In additional experiments, however, we have found that the biogenesis and possibly the structure of the region incorporating m2 and the sequence between m2 and m3 involves more than simple cotranslational integration. These experiments are illustrated in Figure 3. In Figure 3A, we illustrate the results of experiments where the NKCC1 sequence inserted into pEGFP-β was truncated at a series of points, one at the end of m2 (L327) and others at several places in the loop between m2 and m3 (G340, I347, and G357). The construct truncated at the end of m2 (L327) is relatively strongly glycosylated (~70%), indicating that m2 *by itself* does not have sufficient stop transfer activity to be integrated efficiently into the ER membrane. The blots for G340, I347, and G357 are complicated by the appearance of a lower molecular-weight band migrating at ~30 kDa (indicated by an arrow in Figure 3A). Because these bands are recognized by the anti-GFP antibody, they presumably represent proteolytic products containing the N-terminal ends of the respective fusion proteins.

To determine the percent glycosylation of the truncation mutants G340, I347, and G357 and thereby their conformation in the membrane, we must know whether the 30 kDa proteolytic products are derived from glycosylated or unglycosylated fusion proteins. To answer this question, we probed blots of these same membrane fractions with an antibody directed against the fragment of the β subunit of the gastric ATPase used as our glycosylation tag (see the Materials and Methods) to see if we could detect the opposite (C-terminal) ends of these cleaved recombinant proteins. In Figure 3B, we demonstrate that in membranes from HEK293T cells transfected with the construct L327 this antibody recognizes the full-length glycosylated and unglycosylated forms of this recombinant protein as does the antibody directed against EGFP (left panel of Figure 3A). However, in cells transfected with G357, the β-subunit antibody not only detects the full-length G357 construct but also bands migrating at ~46 and ~34 kDa in samples not treated (−)

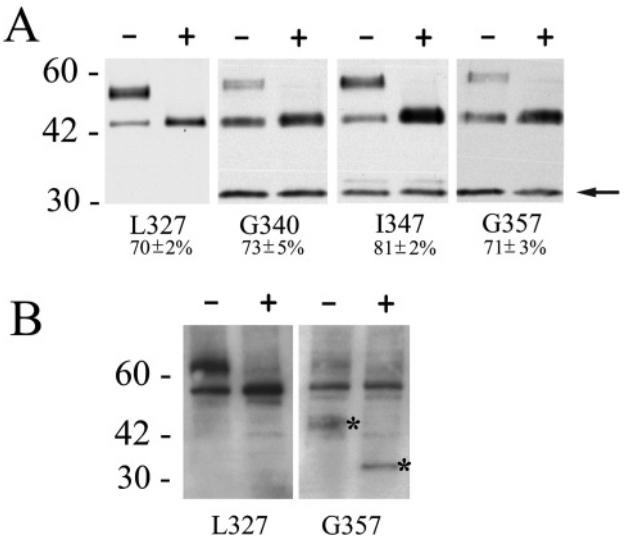

FIGURE 3: Behavior of constructs truncated in the loop between m2 and m3. (A) Typical Western blots of membrane fractions prepared from HEK-293T cells transfected with the truncation mutants indicated. Experimental procedures and analysis were as described for Figure 2A. In the analysis of percent glycosylation, the ~30 kDa proteolytic product (arrow) was assumed to be the component of the glycosylated band (see the text for an explanation). (B) Western blots of membrane fractions prepared from HEK-293T cells transfected with the truncation mutants indicated and probed with an antibody recognizing the C-terminal glycosylation tag (see the Materials and Methods for details). Note that the apparent molecular weights of the full-length glycosylated and unglycosylated fusion proteins are higher when probed in denatured (boiled) samples in this panel than in nondenatured (unboiled) samples probed with the anti-GFP antibody in A. The use of boiled versus unboiled samples was necessary, owing to the specificity of the respective antibodies (see the Materials and Methods).

and treated (+) with PNGase F, respectively (both bands are indicated by asterisks in Figure 3B). These bands, like the 30 kDa proteolytic product recognized by the anti-EGFP antibody, are not seen in blots of membranes from cells transfected with L327 (Figure 3B). We conclude therefore that the ~46 and ~34 kDa bands detected by the β-subunit antibody in all likelihood represent the C-terminal end of the proteolytically cleaved G357 fusion proteins. Because the unglycosylated ~34 kDa band is undetectable without PNGase treatment (right panel of Figure 3B), we also conclude that most of the 30 kDa proteolytic products observed in Figure 3A are derived from *glycosylated* fusion proteins. Accordingly, in the calculations of percent glycosylated recombinant protein indicated below each panel in Figure 3A, we have treated the ~30 kDa band as a component of the glycosylated band. We speculate that the cleavage of the fusion proteins G340, I347, and G357 documented in Figure 3 may be due to luminal signal peptidase. Interestingly, the extent to which these recombinant proteins are cleaved is highly dependent upon the length of the NKCC1 sequence following m2. For example, there is a clear difference between the amount of cleaved product observed with the constructs G340 and I347 (Figure 3A), which only differ by seven amino acids of NKCC1 sequence. There is also a significant proteolytic cleavage of G357 (Figure 3A) and little if any cleavage of I362 (Figure 2A), which is only five amino acids longer. Additional experiments to examine the significance and specificity of these effects are beyond the scope of the present paper, and we have not examined these issues further.

When the results of Figure 3 are combined with those obtained with I362 (Figure 2A), we conclude that m2 does not integrate efficiently into the membrane until after the synthesis of the loop between m2 and m3. In this regard, it has been well-documented that flanking downstream sequence can play a significant role in constraining hydrophobic regions to integrate into the membrane (*17*−*19*). This can, for example, be the result of the presence of charged amino acids or secondary structure in the flanking region that makes it impossible for this sequence to pass through the translocon pore, thereby anchoring it on the cytosolic side of the membrane. In fact, the loop between m2 and m3 does contain several charged amino acids (R339, R349, and E354); however, these residues by themselves do not seem to play an important part in the behavior of m2 because they are all included in the construct G357 in which m2 is still apparently not efficiently integrated into the membrane (Figure 3A). The loop between m2 and m3 is one of the most well-conserved regions in the NKCC1 gene family, and several groups have demonstrated that it plays an important role in determining ion-transport affinities (*29*, *30*). It has been speculated (*30*) that this region forms a part of a pore-like ion-binding pocket within the membrane similar to that observed in a number of ion channels. Our results do not address the conformation of this loop; however, they do indicate an important role of this well-conserved region in the NKCC1 structure and biogenesis.

Membrane Integration of m5, m6, m7, and m8. The data shown in parts A and B of Figure 4 illustrate the results of a series of experiments where the NKCC1 insert in pEGFP-β was truncated after m5 (T444), at two points after m6 (G495 and G512), at two points after m7 (G532 and S556), and at three points after m8 (S612, F632, and I647). The mutant truncated after m5 (T444) is highly glycosylated (~80%), indicating that m5 is recognized by the translocon as a signal anchor sequence downstream of m4 and integrated into the ER membrane in a N_{cyt}/C_{lum} orientation in this construct. However, both the mutant truncated immediately after m6 (G495) and the one truncated at the end of the loop between m6 and m7 (G512) are also relatively highly glycosylated, indicating that m6 does not have sufficient stop transfer activity to integrate efficiently into the membrane in these fusion proteins. In contrast, both of the mutants truncated after m7 (G532 and S556) are only weakly glycosylated (~30%). These data suggest that the dominant topology of the fusion proteins truncated after m7 is the one illustrated in Figure 4D, where m6 is left out of the membrane on the luminal side of the ER and m7 has a N_{lum}/C_{cyt} (stop transfer) orientation, opposite to its proposed orientation in the final folded protein.

When the NKCC1 sequence in pEGFP-β is truncated at S612 immediately after m8, the corresponding fusion protein is highly glycosylated (~70%), indicating that m8 by itself acts as a signal anchor sequence downstream of m7. However, as the insert in pEGFP-β is extended to include more of the loop between m8 and m9 (F632 and I647), the glycosylation of the fusion protein is reduced to ~30%, indicating that in these latter two constructs this loop is predominantly located on the cytoplasmic side of the ER. Thus, the loop between m8 and m9, like the loop between

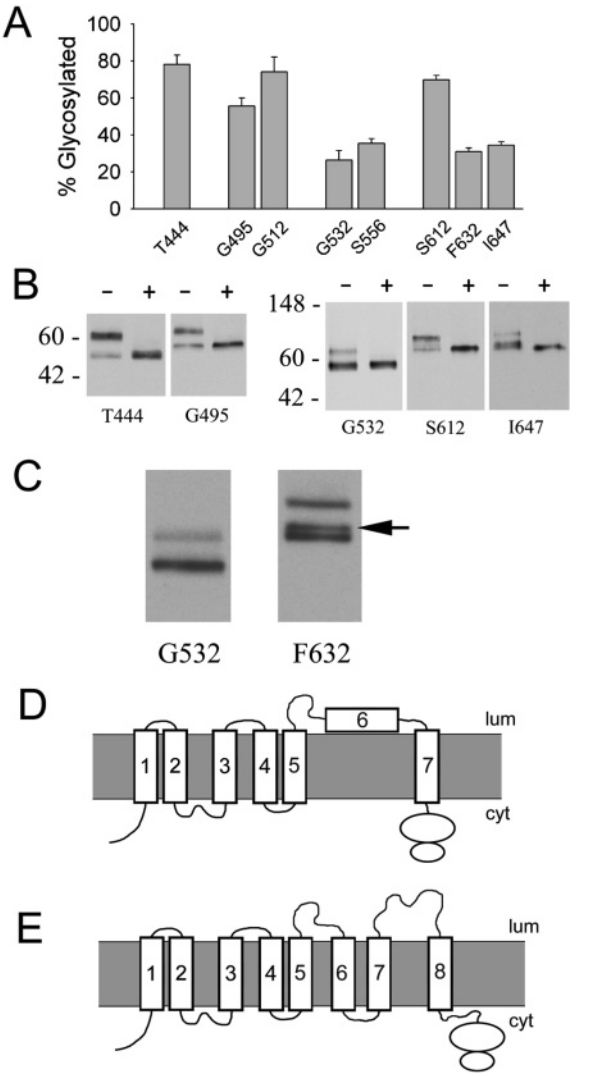

FIGURE 4: Membrane integration of m5−m8 of NKCC1. (A) Percent glycosylated recombinant protein for the constructs indicated was calculated as described in the caption of Figure 2. (B) Typical Western blots of membrane fractions prepared from HEK-293T cells transfected with some of the truncation mutants included in A. Membranes were treated with (+) or without (−) PNGase F as indicated. (C) Western blots of "unprocessed" membranes prepared from HEK-293T cells transfected with G532 (truncated after m7) and F632 (truncated after m8). These membranes were prepared as described in the Materials and Methods but not "processed" for the treatment with or without PNGase F. The arrow indicates a band apparently resulting from the glycosylation of the native glycosylation sites of NKCC1 located in the extracellular loop between m7 and m8. (D) Schematic representation of the topology of constructs truncated after m7 (see the text). (E) Schematic representation of the topology of m1−m8 of NKCC1. See the text for a discussion.

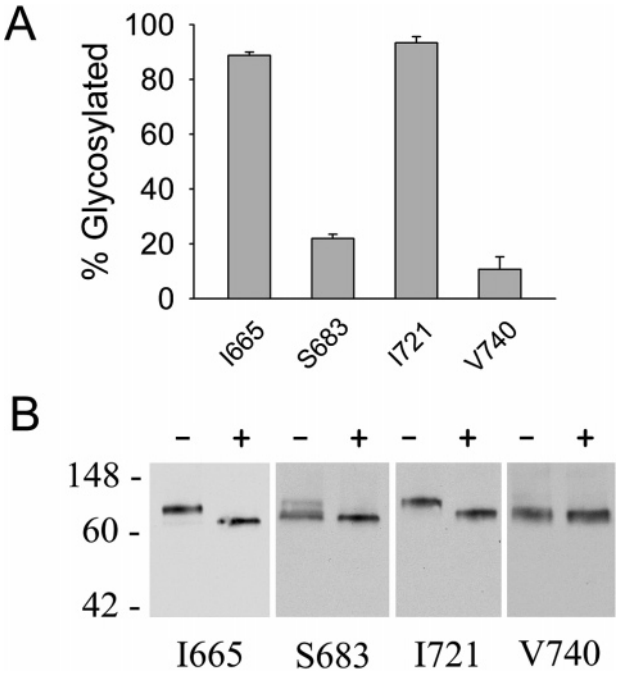

FIGURE 5: Membrane integration of m9−m12 of NKCC1. (A) Percent glycosylated recombinant protein for the constructs indicated was calculated as described in the caption of Figure 2. (B) Typical Western blots of membrane fractions prepared from HEK-293T cells transfected with the truncation mutants analyzed in A. Membranes were treated with (+) or without (−) PNGase F as indicated.

m2 and m3, must incorporate a topogenic signal that constrains it to be retained in the cytoplasm.

The above results indicate that the integration of hydrophobic regions m6, m7, and m8 into the membrane is a complex process that is dependent upon the presence of the loop between m8 and m9. The location of this loop in the cytoplasm together with the fact that the native glycosylation sites in NKCC1 lie in the loop between m7 and m8 (which therefore must be located in ER lumen) requires that m8 spans the membrane in a N_{lum}/C_{cyt} orientation. The glycosylation of one or both of these native sites can be seen in "unprocessed" membranes prepared from cells transfected with F632 in Figure 4C (arrow). For reasons that are unclear to us, the "processing" of the membrane fraction for deglycosylation (see the Materials and Methods), whether actually treated with PNGase F or not, results in a broadening of the bands that we observe on Western blots. This, together with the fact that the increase in apparent molecular weight associated with glycosylation of the native glycosylation sites is small, makes this phenomenon difficult to discern on the typical Western blots of processed membranes that we present here (e.g., for I647 in Figure 4B).

Only two topological arrangements for m6 and m7 are consistent with the N_{lum}/C_{cyt} orientation of m8 and the N_{cyt}/C_{lum} orientation of m5 (see above). One of these is illustrated in Figure 4E; here, m6 and m7 are integrated into the membrane as typically proposed for members of the CCC transporter family. The second possibility is that both m6 and m7 are completely left out of the membrane on the luminal side of the ER. Although our results do not definitively exclude this latter model, we would argue that it is very unlikely, owing to the hydrophobic natures of both of these segments (Figure 1A), particularly that of m7, which is well above the threshold for membrane insertion proposed by Kyte and Doolittle (dashed line in Figure 1A). Indeed, m7 is apparently capable of membrane integration as seen in the constructs G532 and S556 (parts A and D of Figure 4). Furthermore, there is good evidence that both m6 and m7 are involved in the ion-transport event (*31*, *32*), consistent with their location within the lipid bilayer.

Membrane Integration of m9, m10, m11, and m12. The results shown in Figure 5A confirm previous suggestions (*33*, *34*) and experimental evidence (*12*) that the broad hydrophobic regions m9−m10 and m11−m12 of NKCC1

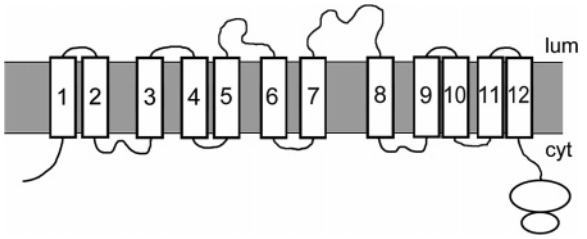

FIGURE 6: Proposed topology of the central hydrophobic domain of NKCC1.

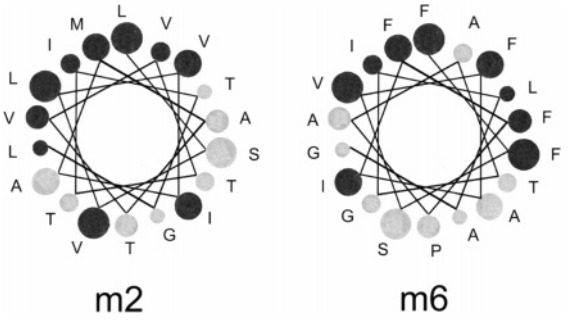

FIGURE 7: Helical wheel representation of regions m2 and m6 of NKCC1. Hydrophobic residues are darkly shaded. The view is from the N terminus in each case. The helical wheel was drawn with the aid of a program made available by Dr. Charles M. Grisham (University of Virginia) at http://cti.itc.virginia.edu/~cmg/Demo/wheel/wheelApp.html.

(Figure 1A) each form tight hairpin-like structures consisting of two MSSs each. As illustrated in Figure 5A, our constructs truncated at the ends of m9 (I665) and m11 (I721) are highly glycosylated (~90%) and those truncated at the ends of m10 (S683) and m12 (V740) are poorly glycosylated (~20 and 10%, respectively). Thus, m9 and m11 act independently as signal anchor sequences, and m10 and m12 act as their respective stop transfers. The structural and/or functional significance of these two tightly spaced hairpin-like structures that are characteristic of the CCCs is presently unknown.

CONCLUDING REMARKS

The results presented here support our earlier conclusions (*12*) and the previous conjectures of others (*33*−*35*) regarding the 12 MSS transmembrane topology of NKCC1; a schematic model of the proposed topology of this region is shown in Figure 6. Our data also reveal several unexpected results concerning NKCC1 biogenesis, namely, that MSSs 2 and 6 apparently do not integrate efficiently into the membrane in the absence of the downstream sequence. Interestingly, when the amino acids in both of these regions are plotted in a helical wheel format (Figure 7), it is clear that most of their hydrophobic residues (shaded dark gray in Figure 7) are located on one helical face. This polarized hydrophobicity distribution could be responsible for their inability to integrate efficiently into the membrane independently. Indeed, Heinrich et al. (*20*) have proposed that one of the functions of the translocon channel is to retain amphipathic MSSs of this type until they can assemble with other MSSs into structures that shield their hydrophilic surfaces before they are released and integrated into the lipid environment.

As we have discussed above and elsewhere (*21*), the truncation mutant approach employed here has several significant advantages over earlier methods for studying transmembrane topology and biogenesis. Nevertheless, this method still relies on interpreting the way that genetically engineered recombinant proteins interact with the membrane integration machinery. Our ultimate understanding of the structure and structure/function relationships of NKCC1 will rely on more direct structural measurements such as those arising from crystallographic studies.

ACKNOWLEDGMENT

We thank Dr. Bruce J. Baum for many useful discussions during the course of this work.

REFERENCES

1. Haas, M., and Forbush, B., III (2000) The Na−K−Cl cotransporter of secretory epithelia, *Annu. Rev. Physiol. 62*, 515−534.
2. Gamba, G. (2005) Molecular physiology and pathophysiology of electroneutral cation-chloride cotransporters, *Physiol. Rev. 85*, 423−493.
3. Delpire, E., and Mount, D. B. (2002) Human and murine phenotypes associated with defects in cation-chloride cotransport, *Annu. Rev. Physiol. 64*, 803−843.
4. Flagella, M., Clarke, L. L., Miller, M. L., Erway, L. C., Giannella, R. A., Andringa, A., Gawenis, L. R., Kramer, J., Duffy, J. J., Doetschman, T., Lorenz, J. N., Yamoah, E. N., Cardell, E. L., and Shull, G. E. (1999) Mice lacking the basolateral Na−K−2Cl cotransporter have impaired epithelial chloride secretion and are profoundly deaf, *J. Biol. Chem. 274*, 26946−26955.
5. Delpire, E., Lu, J., England, R., Dull, C., and Thorne, T. (1999) Deafness and imbalance associated with inactivation of the secretory Na−K−2Cl co-transporter, *Nat. Genet. 22*, 192−195.
6. Meyer, J. W., Flagella, M., Sutliff, R. L., Lorenz, J. N., Nieman, M. L., Weber, C. S., Paul, R. J., and Shull, G. E. (2002) Decreased blood pressure and vascular smooth muscle tone in mice lacking basolateral Na^+−K^+−$2Cl^-$ cotransporter, *Am. J. Physiol. 283*, H1846−H1855.
7. Evans, R. L., Park, K., Turner, R. J., Watson, G. E., Nguyen, H. V., Dennett, M. R., Hand, A. R., Flagella, M., Shull, G. E., and Melvin, J. E. (2000) Severe impairment of salivation in Na^+/K^+/$2Cl^-$ cotransporter (NKCC1)-deficient mice, *J. Biol. Chem. 275*, 26720−26726.
8. Kaneko, H., Putzier, I., Frings, S., Kaupp, U. B., and Gensch, T. (2004) Chloride accumulation in mammalian olfactory sensory neurons, *J. Neurosci. 24*, 7931−7938.
9. Pace, A. J., Lee, E., Athirakul, K., Coffman, T. M., O'Brien, D. A., and Koller, B. H. (2000) Failure of spermatogenesis in mouse lines deficient in the Na^+−K^+−$2Cl^-$ cotransporter, *J. Clin. Invest. 105*, 441−450.
10. Sung, K. W., Kirby, M., McDonald, M. P., Lovinger, D. M., and Delpire, E. (2000) Abnormal GABAA receptor-mediated currents in dorsal root ganglion neurons isolated from Na−K−2Cl cotransporter null mice, *J. Neurosci. 20*, 7531−7538.
11. Grubb, B. R., Lee, E., Pace, A. J., Koller, B. H., and Boucher, R. C. (2000) Intestinal ion transport in NKCC1-deficient mice, *Am. J. Physiol. 279*, G707−G718.
12. Gerelsaikhan, T., and Turner, R. J. (2000) Transmembrane topology of the secretory Na^+−K^+−$2Cl^-$ cotransporter NKCC1 studied by in vitro translation, *J. Biol. Chem. 275*, 40471−40477.
13. Forbush, B., Payne, J. A., Xu, J. C., Biemesderfer, D., and Isenring, P. (1995) *Abstracts of the International Society of Nephrology*, American Physiological Society, Bethesda, MD.
14. Paredes, A., Plata, C., Rivera, M., Moreno, E., Vazquez, N., Munoz-Clares, R., Hebert, S. C., and Gamba, G. (2006) Activity of the renal Na^+−K^+−$2Cl^-$ cotransporter is reduced by mutagenesis of N-glycosylation sites: Role for protein surface charge in Cl^- transport, *Am. J. Physiol. 290*, F1094−F1102.
15. Hoover, R. S., Poch, E., Monroy, A., Vazquez, N., Nishio, T., Gamba, G., and Hebert, S. C. (2003) N-Glycosylation at two sites critically alters thiazide binding and activity of the rat thiazide-sensitive Na^+:Cl^- cotransporter, *J. Am. Soc. Nephrol. 14*, 271−282.
16. Johnson, A. E., and van Waes, M. A. (1999) The translocon: A dynamic gateway at the ER membrane, *Annu. Rev. Cell Dev. Biol. 15*, 799−842.

17. Turner, R. J. (2003) Understanding the biogenesis of polytopic integral membrane proteins, *J. Membr. Biol. 192*, 149−157.
18. White, S. H., and von Heijne, G. (2004) The machinery of membrane protein assembly, *Curr. Opin. Struct. Biol. 14*, 397−404.
19. Higy, M., Junne, T., and Spiess, M. (2004) Topogenesis of membrane proteins at the endoplasmic reticulum, *Biochemistry 43*, 12716−12722.
20. Heinrich, S. U., Mothes, W., Brunner, J., and Rapoport, T. A. (2000) The Sec61p complex mediates the integration of a membrane protein by allowing lipid partitioning of the transmembrane domain, *Cell 102*, 233−244.
21. Dohke, Y., and Turner, R. J. (2002) Evidence that the transmembrane biogenesis of aquaporin 1 is cotranslational in intact mammalian cells, *J. Biol. Chem. 277*, 15215−15219.
22. Dohke, Y., Oh, Y. S., Ambudkar, I. S., and Turner, R. J. (2004) Biogenesis and topology of the transient receptor potential Ca^{2+} channel TRPC1, *J. Biol. Chem. 279*, 12242−12248.
23. Moore-Hoon, M. L., and Turner, R. J. (1998) Molecular and topological characterization of the rat parotid $Na^+-K^+-2Cl^-$ cotransporter 1, *Biochim. Biophys. Acta 1373*, 261−269.
24. Bamberg, K., and Sachs, G. (1994) Topological analysis of H^+,K^+-ATPase using in vitro translation, *J. Biol. Chem. 269*, 16909−16919.
25. Bayle, D., Weeks, D., and Sachs, G. (1995) The membrane topology of the rat sarcoplasmic and endoplasmic reticulum calcium ATPases by in vitro translation scanning, *J. Biol. Chem. 270*, 25678−25684.
26. Bayle, D., Weeks, D., and Sachs, G. (1997) Identification of membrane insertion sequences of the rabbit gastric cholecystokinin-A receptor by in vitro translation, *J. Biol. Chem. 272*, 19697−19707.
27. Denzer, A. J., Nabholz, C. E., and Spiess, M. (1995) Transmembrane orientation of signal-anchor proteins is affected by the folding state but not the size of the N-terminal domain, *EMBO J. 14*, 6311−6317.
28. Goder, V., and Spiess, M. (2001) Topogenesis of membrane proteins: Determinants and dynamics, *FEBS Lett. 504*, 87−93.
29. Gimenez, I., Isenring, P., and Forbush, B. (2002) Spatially distributed alternative splice variants of the renal Na−K−Cl cotransporter exhibit dramatically different affinities for the transported ions, *J. Biol. Chem. 277*, 8767−8770.
30. Gagnon, E., Bergeron, M. J., Brunet, G. M., Daigle, N. D., Simard, C. F., and Isenring, P. (2004) Molecular mechanisms of Cl^- transport by the renal $Na^+-K^+-Cl^-$ cotransporter. Identification of an intracellular locus that may form part of a high affinity Cl^--binding site, *J. Biol. Chem. 279*, 5648−5654.
31. Dehaye, J. P., Nagy, A., Premkumar, A., and Turner, R. J. (2003) Identification of a functionally important conformation-sensitive region of the secretory $Na^+-K^+-2Cl^-$ cotransporter (NKCC1), *J. Biol. Chem. 278*, 11811−11817.
32. Isenring, P., Jacoby, S. C., Chang, J., and Forbush, B. (1998) Mutagenic mapping of the Na−K−Cl cotransporter for domains involved in ion transport and bumetanide binding, *J. Gen. Physiol. 112*, 549−558.
33. Xu, J. C., Lytle, C., Zhu, T. T., Payne, J. A., Benz, E., Jr., and Forbush, B., III (1994) Molecular cloning and functional expression of the bumetanide-sensitive Na−K−Cl cotransporter, *Proc. Natl. Acad. Sci. U.S.A. 91*, 2201−2205.
34. Payne, J. A., Xu, J. C., Haas, M., Lytle, C. Y., Ward, D., and Forbush, B., III (1995) Primary structure, functional expression, and chromosomal localization of the bumetanide-sensitive Na−K−Cl cotransporter in human colon, *J. Biol. Chem. 270*, 17977−17985.
35. Delpire, E., Rauchman, M. I., Beier, D. R., Hebert, S. C., and Gullans, S. R. (1994) Molecular cloning and chromosome localization of a putative basolateral $Na^+-K^+-2Cl^-$ cotransporter from mouse inner medullary collecting duct (mIMCD-3) cells, *J. Biol. Chem. 269*, 25677−25683.
36. Kyte, J., and Doolittle, R. F. (1982) A simple method for displaying the hydropathic character of a protein, *J. Mol. Biol. 157*, 105−132.

BI061126X